Chemical Engineering Journal 217 (2013) 300–309

Contents lists available at SciVerse ScienceDirect

Chemical Engineering Journal

journal homepage: www.elsevier.com/locate/cej

Ir/Pt-HZSM5 for *n*-pentane isomerization: Effect of Si/Al ratio and reaction optimization by response surface methodology

H.D. Setiabudi [a], A.A. Jalil [a], S. Triwahyono [b,c,*], N.H.N. Kamarudin [a], R. Jusoh [a]

[a] Institute of Hydrogen Economy, Faculty of Chemical Engineering, Universiti Teknologi Malaysia, 81310 UTM Johor Bahru, Johor, Malaysia
[b] Department of Chemistry, Faculty of Science, Universiti Teknologi Malaysia, 81310 UTM Johor Bahru, Johor, Malaysia
[c] Ibnu Sina Institute for Fundamental Science Studies, Universiti Teknologi Malaysia, 81310 UTM Johor Bahru, Johor, Malaysia

HIGHLIGHTS

- High activity of catalyst was observed for Ir/Pt-HZSM5 with Si/Al ratio of 23.
- Isomerization of *n*-pentane over Ir/Pt-HZSM5 was optimized by RSM.
- The largest effect on *n*-pentane isomerization was reaction temperature.
- The least important effect on *n*-pentane isomerization was *F*/*W*.
- The yield of isopentane could reach 61.9% under the optimum conditions.

GRAPHICAL ABSTRACT

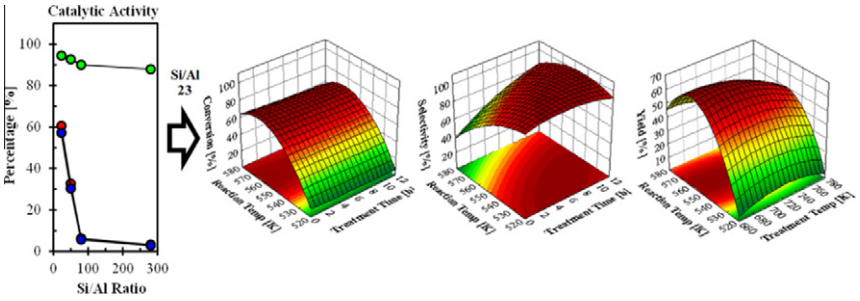

ARTICLE INFO

Article history:
Received 21 September 2012
Received in revised form 23 November 2012
Accepted 3 December 2012
Available online 10 December 2012

Keywords:
Ir/Pt-HZSM5
n-Pentane isomerization
Si/Al ratio
Strong acid sites
Response surface methodology (RSM)

ABSTRACT

The effects of Si/Al ratio on the properties of Ir/Pt-HZSM5 and *n*-pentane isomerization were studied. XRD results indicated that the increasing Si/Al ratio increased the percentage crystallinity of the catalysts, whereas, FTIR results showed that the increasing Si/Al ratio decreased the number of strong Brönsted and Lewis acid sites which led to decrease the catalytic activity towards *n*-pentane isomerization. Ir/Pt-HZSM5 with Si/Al ratio of 23 showed highest activity towards *n*-pentane isomerization, and the operating condition was further optimized by using response surface methodology (RSM). The RSM experiments were designed by using face-centered central composite design (FCCCD) by applying 2^4 factorial points, 8 axial points and 2 replicates, with three response variables (*n*-pentane conversion, isopentane selectivity and isopentane yield). The Pareto chart indicated that the reaction temperature have largest effect for all responses. The optimum condition of *n*-pentane isomerization over Ir/Pt-HZSM5 was at treatment temperature of 723 K, treatment time of 6 h, reaction temperature of 548 K and *F*/*W* of 500 ml g^{-1} min^{-1} in which the predicted value for the *n*-pentane conversion, isopentane selectivity and isopentane yield was 63.0%, 98.2% and 61.9%, respectively.

1. Introduction

Catalyzed isomerization of *n*-alkane is one of the important processes in petroleum refining to modify the octane number of gasoline. Isomerization reaction generally takes place over bifunctional catalyst containing metallic sites for hydrogenation/dehydrogenation and acid sites for skeletal isomerization. Several types of bifunctional heterogeneous catalyst, consisting of metal supported on metal oxides [1–3], mesoporous [4] and microporous [5,6] materials have been widely explored for the isomerization process [7]. In addition, the introduction of noble metal or transition metals to the catalysts and the presence of hydrogen in the gas phase markedly improved the activity and stability of the

* Corresponding author at: Ibnu Sina Institute for Fundamental Science Studies, Universiti Teknologi Malaysia, 81310 UTM Johor Bahru, Johor, Malaysia. Tel.: +60 7 5536076; fax: +60 7 5536080.
E-mail address: sugeng@utm.my (S. Triwahyono).

1385-8947/$ - see front matter © 2012 Elsevier B.V. All rights reserved.
http://dx.doi.org/10.1016/j.cej.2012.12.011

catalyst [8]. In particular, platinum metal has been widely used as a promoter for heterogeneous catalyst [6–10] and has drawn a great interest in isomerization process [6,7].

In recent years, bimetallic heterogeneous catalysts have attracted an increasing interest due to their capability to improve the activity, stability and selectivity of the catalysts. In particular, bimetallic catalysts composed by iridium and platinum were found to be active and stable for isomerization. Iridium species are well known co-promoter that are added to catalysts because of their stability during the coke removal process [11,12]. Several research groups have reported that the introduction of iridium as co-promoter enhanced the catalytic activity of monometallic catalysts and decreased the formation of coke [13–16]. In our previous assignment, we have reported the effect of iridium on Pt-HZSM5 for isomerization of *n*-pentane [15,16]. Pt-HZSM5 with 0.1 wt% iridium loading was found as the most potential catalyst for *n*-pentane isomerization. The presence of 0.1 wt% iridium increased the number of strong acid sites and active protonic acid sites originated from molecular hydrogen via hydrogen spillover phenomenon for *n*-pentane isomerization. Moreover, iridium oxide bonded to perturbed silanol groups inhibited the formation of hydroxyl groups from molecular hydrogen at 3680, 3600 and 3380 cm^{-1}, where those hydroxyl groups may participate in the enhancement of the cracking reaction.

In this report, we have studied the influence of Si/Al ratio on the properties of Ir/Pt-HZSM5 catalyst, and consequently the effect of acidic strength on the performance of Ir/Pt-HZSM5 in *n*-pentane isomerization. Furthermore, the optimum condition of *n*-pentane isomerization over Ir/Pt-HZSM5 was identified by response surface methodology (RSM). The formation of coke deposits on the surface of Ir/Pt-HZSM5 will also be discussed.

2. Experimental

2.1. Catalyst preparation

A commercial HZSM5 (Zeolyst International) with Si/Al atomic ratio of 23, 50, 80 and 280 were used as supports. Ir/Pt-HZSM5 was prepared according to the method described in previous report [15]. In brief, Pt-HZSM5 was prepared by incipient wetness impregnation of HZSM5 with an aqueous solution containing the requisite quantity of $H_2PtCl_6{\cdot}H_2O$ (Merck) to obtained 0.1 wt% Pt, followed by drying at 383 K overnight and calcination at 823 K for 3 h in air. The prepared Pt-HZSM5 was then impregnated with aqueous solution of $IrCl_3{\cdot}3H_2O$ (Merck) to obtained bimetallic Ir/Pt-HZSM5, followed by drying at 383 K overnight and calcination at 823 K for 3 h in air. The content of Ir was adjusted to 0.1 wt%.

2.2. Catalyst characterization

The crystalline structure of the catalyst was confirmed by X-ray diffraction (XRD) recorded on a powder diffractometer (40 kV, 40 mA) using Cu Kα radiation source in the range of $2\theta = 2–50^\circ$. Percentage crystallinity was calculated using the average peak intensity of the peaks at $2\theta = 7.9^\circ$ and 8.9°, in which Ir/Pt-HZSM5 with Si/Al atomic ratio of 280 was used as a reference.

Fourier Transform Infra Red (FTIR) measurements were carried out with Agilent Cary 640 FTIR Spectrometer. The catalyst was prepared as a self-supported wafer and activated under hydrogen flow at 673 K for 3 h, followed by outgassing at 673 K for 3 h [17]. The activated catalyst was then exposed to 2 Torr of 2,6-lutidine at room temperature for 30 min, followed by outgassing at 473 K for 30 min. The spectra were recorded at room temperature.

2.3. Isomerization of n-pentane

The isomerization of *n*-pentane was performed under hydrogen atmosphere in a microcatalytic pulse reactor according to the method described in the literatures [18]. Prior to the reaction, 0.2 g of catalyst was treated in a flow of oxygen (F_{Oxygen} = 100 ml/min) for 1 h, followed by hydrogen ($F_{Hydrogen}$ = 100 ml/min) for 3 h at 673 K and cooled down to 548 K in a hydrogen stream. A dose of *n*-pentane (43 μmol) was injected over the activated catalyst, and the products were trapped at 77 K before flash-evaporation into an online 6090 N Agilent gas chromatograph equipped with HP-5 Capillary Column and FID detector. The intervals between each pulse injection were kept constant at 20 min. Since all catalysts reached steady state condition within 7 pulses (140 min), results at 7 pulses were used. For the research surface methodology (RSM) analysis, catalytic reactions were performed with different reaction variables based on the face-centred central composite design (FCCCD) method.

The conversion of *n*-pentane ($X_{n\text{-}pentane}$) was calculated according to the following equation:

$$X_{n-pentane}\ (\%) = \frac{\sum [C]_i}{\sum [C]_i + [C]_{residualn\text{-}pentane}} \times 100 \quad (1)$$

where $[C]_i$ and $[C]_{residual\ n\text{-}pentane}$ are mol number for particular product and for residual *n*-pentane which is calculating based on the Scott hydrocarbon calibration standard gas (Air Liquide America Specialty Gases LLC). The selectivity ($S_{isopentane}$) and yield ($Y_{isopentane}$) to isopentane was calculated according to Eqs. (2) and (3), respectively.

$$S_{isopentane}\ (\%) = \frac{[C]_{isopentane}}{\sum [C]_i} \times 100 \quad (2)$$

$$Y_{isopentane}\ (\%) = \frac{X_{n-pentane} \times S_{isopentane}}{100} \quad (3)$$

2.4. Experimental design and optimization

In this study, statistical analysis of *n*-pentane isomerization, isopentane selectivity and isopentane yield in isomerization of *n*-pentane was performed using Statsoft Statistica 8.0 software. The FCCCD was used to study the interaction of process variables and to predict the optimum process condition for *n*-pentane isomerization by applying RSM. Independent variables considered important were treatment temperature (X_1), treatment time (X_2), reaction temperature (X_3) and flow of hydrogen over weight of catalyst, F/W (X_4). Treatment temperature is referred to the temperature used during the treatment process prior to the reaction, while treatment time is referred to the time used during the treatment process under hydrogen stream prior to the reaction. The range and coded level of the isomerization process variables studied are listed in Table 1. The independent variables were coded to the (−1, 1) interval where the low and high levels were coded as −1 and +1, respectively. According to FCCCD, the total number of experiments conducted is 26 with 2^4 factorial points, 8 axial points and 2 replicates at the center points. The *n*-pentane conversion (Y_1), isopentane selectivity (Y_2) and isopentane yield (Y_3) were

Table 1
Coded levels for independent variables used in the experimental design.

Independent variables	Symbol	Coded levels		
		−1	0	+1
Treatment temperature (K)	X_1	673	723	773
Treatment time (h)	X_2	1	6	11
Reaction temperature (K)	X_3	523	548	573
F/W (ml g^{-1} min^{-1})	X_4	475	500	525

taken as the response of the design experiment. The experimental design and corresponding results of three responses are listed in Table 2.

The full quadratic models for *n*-pentane conversion, isopentane selectivity and isopentane yield are given as the following equation:

$$Y_i = \beta_o + \beta_1 X_1 + \beta_2 X_2 + \beta_3 X_3 + \beta_4 X_4 + \beta_{12} X_1 X_2 + \beta_{13} X_1 X_3 + \beta_{14} X_1 X_4 + \beta_{23} X_2 X_3 + \beta_{24} X_2 X_4 + \beta_{34} X_3 X_4 + \beta_{11} X_1^2 + \beta_{22} X_2^2 + \beta_{33} X_3^2 + \beta_{44} X_4^2 \quad (4)$$

where Y_i is the predicted response i whilst X_1, X_2, X_3 and X_4 are the coded form of independent variables. The term β_o is the offset term; β_1, β_2, β_3 and β_4 are the linear terms; β_{11}, β_{22}, β_{33} and β_{44} are the quadratic terms; and β_{12}, β_{13}, β_{14}, β_{23}, β_{24} and β_{34} are the interaction terms.

The equation model was tested with the analysis of variance (ANOVA) with 5% level of significant. The ANOVA was used to checking the significance of the second-order models and it is determined by *F*-value. Generally, the calculated *F*-value should be greater than tabulated *F*-value to reject the null hypothesis, where all the regression coefficients are zero. The calculated *F*-value is defined as the following equation:

$$F\text{-value} = \frac{MS_{SSR}}{MS_{SSE}} \quad (5)$$

where MS_{SSR} and MS_{SSE} are mean of square regression and mean of square residual. The MS_{SSR} and MS_{SSE} were obtained by dividing sum of squares (SSR) and sum of residual (SSE) over degree of freedom (DF), respectively. Meanwhile, tabulated *F*-value was obtained from *F* distribution based on DF for regression and residual, respectively at a specific level of significance, α-value [19].

3. Results and discussion

3.1. Effect of Si/Al ratio

Different Si/Al ratio (23, 50, 80 and 280) of Ir/Pt-HZSM5 catalysts were used to study the influence of Si/Al ratio, and consequently the effect of acidic strength on the performance of Ir/Pt-HZSM5 in *n*-pentane isomerization.

Fig. 1A shows the XRD patterns of Ir/Pt-HZSM5 catalysts with different Si/Al ratio. All samples exhibited the intense signal in the range of 2θ = 7–10° and 22–25° which were identified as reflections of the HZSM5 zeolite [18,20]. The increase in Si/Al ratio increased the intensity of the XRD peaks, indicating higher silicate framework for sample with lower Al content. Therefore, Fig. 2B shows that the percentage of crystallinity increases with increasing Si/Al ratio. This result indicated that the structural collapse is a function of the Si/Al ratio in which the frameworks with lower aluminum contents are more stable [21]. This result is in agreement with the previous study for HZSM5 zeolite samples reported by Lu et al. [22], where the percentage crystallinity of HZSM5 sample increased by about 36.6% as the Si/Al molar ratio increased from 25 to 150. A similar trend was also observed for Al-MCM-41 samples reported by Reddy and Song [23], in which the samples were synthesized using feed Si/Al ratio of 50, 25 and 12.5. They reported that the decrease in Si/Al ratio resulted in a decrease in the intensity of the main XRD peak, indicating that increasing Al content of the feed hindered crystallization process.

In general, the ratio of Si/Al influences the acidity of the samples due to the variations in the number of framework and extraframework aluminum. In this study, the strength and type of acid sites in the catalysts were qualitatively probed by 2,6-lutidine adsorption monitored by IR spectroscopy. Fig. 2A shows the IR spectra of 2,6-lutidine adsorbed on activated Ir/Pt-HZSM5 catalysts in the region of 1750–1350 cm^{-1}. The spectra were recorded after adsorption of 2,6-lutidine at room temperature, followed by removal of 2,6-lutidine at 473 K. Since the outgassing temperature after 2,6-lutidine adsorption was 473 K, the acid sites under consideration are only strong acid sites that can retain 2,6-lutidine at the outgassing temperature of 473 K and below. All catalysts showed several adsorption bands at 1700, 1680, 1650 and 1640 cm^{-1}, which are associated with the 2,6-lutidinium cations adsorbed on Brönsted acid sites [24]. Whereas, the absorbance bands at 1605, 1585, 1490 and 1460 cm^{-1} corresponded to the Lewis acid sites [24]. The effect of Si/Al ratio on the acidity of the

Table 2
Experimental design and results of the response surface design.

No	Manipulated variables								Responses		
	X_1 (K)	Level	X_2 (h)	Level	X_3 (K)	Level	X_4 (ml/g min)	Level	Conversion Y_1 (%)	Selectivity Y_2 (%)	Yield Y_3 (%)
1	673	−1	1	−1	523	−1	475	−1	17.5	99.7	17.5
2	673	−1	1	−1	523	−1	525	+1	16.8	100.0	16.8
3	673	−1	1	−1	573	+1	475	−1	68.6	76.8	52.7
4	673	−1	1	−1	573	+1	525	+1	67.2	74.9	50.3
5	673	−1	11	+1	523	−1	475	−1	12.8	89.9	11.5
6	673	−1	11	+1	523	−1	525	+1	8.9	90.5	8.1
7	673	−1	11	+1	573	+1	475	−1	64.9	89.4	58.0
8	673	−1	11	+1	573	+1	525	+1	61.7	89.9	55.5
9	773	+1	1	−1	523	−1	475	−1	12.1	90.7	11.0
10	773	+1	1	−1	523	−1	525	+1	9.9	87.0	8.6
11	773	+1	1	−1	573	+1	475	−1	65.6	24.9	16.3
12	773	+1	1	−1	573	+1	525	+1	62.6	23.9	15.0
13	773	+1	11	+1	523	−1	475	−1	11.2	98.1	11.0
14	773	+1	11	+1	523	−1	525	+1	14.3	96.4	13.8
15	773	+1	11	+1	573	+1	475	−1	63.5	80.3	51.0
16	773	+1	11	+1	573	+1	525	+1	59.0	80.3	47.4
17	673	−1	6	0	548	0	500	0	61.0	99.6	60.7
18	773	+1	6	0	548	0	500	0	57.2	89.2	51.0
19	723	0	1	−1	548	0	500	0	67.2	87.4	58.8
20	723	0	11	+1	548	0	500	0	58.3	98.3	57.3
21	723	0	6	0	523	−1	500	0	17.0	100.0	17.0
22	723	0	6	0	573	+1	500	0	64.9	78.7	51.1
23	723	0	6	0	548	0	475	−1	63.8	97.7	62.3
24	723	0	6	0	548	0	525	+1	61.1	97.9	59.8
25	723	0	6	0	548	0	500	0	64.7	99.0	64.0
26	723	0	6	0	548	0	500	0	64.9	99.1	64.3

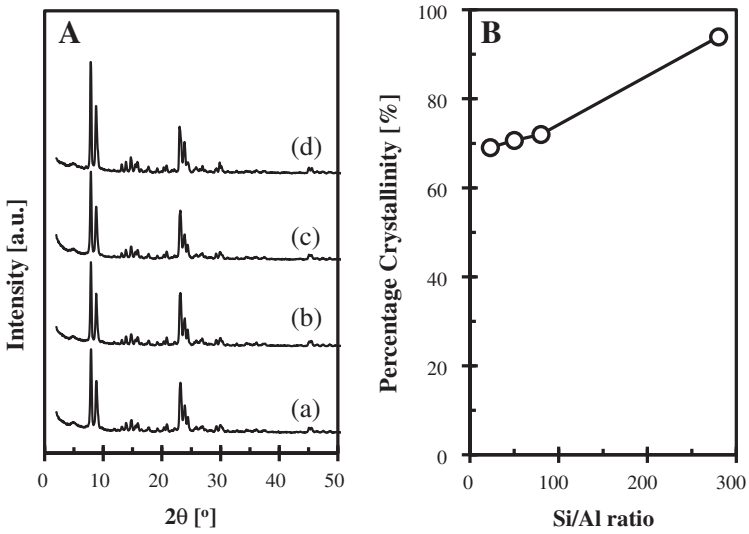

Fig. 1. (A) XRD patterns of Ir/Pt-HZSM5 with Si/Al ratio of (a) 23; (b) 50; (c) 80; (d) 280. (B) Effect of Si/Al ratio on the percentage crystallinity.

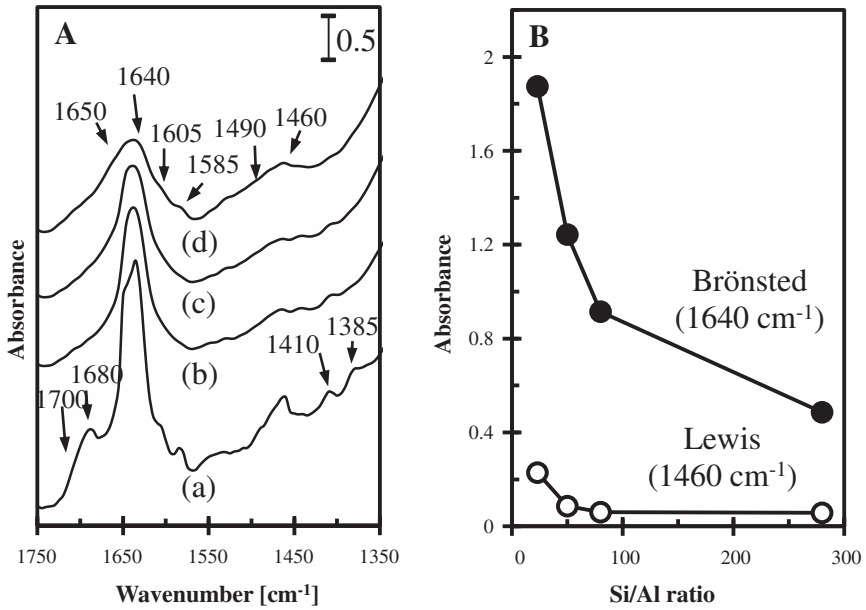

Fig. 2. (A) IR spectra of 2,6-lutidine adsorbed on activated Ir/Pt-HZSM5 with Si/Al ratio of (a) 23; (b) 50; (c) 80; (d) 280 at room temperature followed by removal of 2,6-lutidine at 473 K. (B) Variations in the absorbance of the IR bands for Brönsted and Lewis acid sites after removal of 2,6-lutidine at 473 K.

catalyst are more clearly illustrated in Fig. 2B, in which the absorbance of the IR bands at Brönsted acid sites (1640 cm^{-1}) and Lewis acid sites (1460 cm^{-1}) were plotted as a function of Si/Al ratio. An increase in Si/Al ratio decreased the intensity of band associated with Brönsted acid sites, which is consistent with a decrease in the intensity of the FTIR band assigned to Si(OH)Al at 3610 cm^{-1} (not shown). In addition, the band associated to Lewis acid sites was also decreased with increasing Si/Al ratio. A decrease in the strong acid sites is consistent with the fact that the strong acidity of zeolitic catalyst is attributed the presence of tetrahedral and octahedral Al [25,26]. Similar phenomenon was also observed for ZSM-5 samples as reported by Shirazi et al. [27]. They reported that the intensity of the NH_3-TPD peak associated to strong acid sites decreased as the Si/Al ratio increased. The author suggested that a decrease in the strong acid sites is primarily due to the decrease in extra-framework aluminum content as well as in the framework. Choudhary et al. [28] was also found that the strong acidity of the Ga/HZSM5 catalyst is decreased sharply with increasing Si/Al ratio due to the decrease in the tetrahedral (or framework) Al.

The catalytic activities of Ir/Pt-HZSM5 with different Si/Al ratio were evaluated with respect to *n*-pentane isomerization at 548 K in a microcatalytic pulse reactor. The effect of Si/Al ratio on the conversion of *n*-pentane, selectivity of isopentane and yield of isopentane is shown in Fig. 3. As a general results, the outlet of *n*-pentane reaction consisted of cracking products, isopentane, residual *n*-pentane and higher hydrocarbons. As shown in Fig. 3, the catalytic activity of Ir/Pt-HZSM5 catalysts decreased with the increase of Si/Al ratio, i.e. with decreasing the Al content. This result reveals that the acidity of catalysts is directly associated with the activity of the catalysts towards the isomerization of *n*-pentane. Lower Si/Al ratio denoted the higher number of Al content, thus generates large number of strong acid sites which is favorable for isomerization. As we previously observed [16], the amount of strong Lewis acid sites significantly influenced the formation of protonic acid

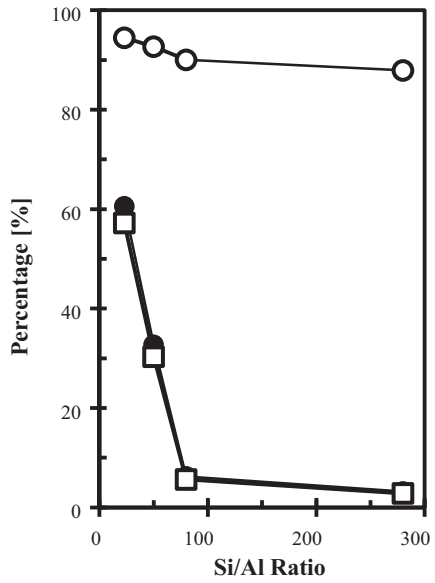

Fig. 3. Effect of Si/Al ratio on the (•) conversion of *n*-pentane, (○) selectivity of isopentane and (□) yield of isopentane.

sites originating from molecular hydrogen, which are required in the isomerization of *n*-pentane over Ir/Pt-HZSM5 catalyst.

The effects of Si/Al ratio on the catalytic performance of zeolite-based catalysts in the isomerization of *n*-alkanes have reported by several research groups. In general, a decrease in the Si/Al ratio means an increase in the aluminum content and, therefore, resulted to an increase in the acid density of the catalyst. De Lucas et al. [29] found that the Si/Al ratio played an important role in the catalytic activity of *n*-octane isomerization over platinum and palladium beta zeolite-based catalysts. An increased in the Si/Al ratio resulted to a decreased in the acid sites density and leading to a low *n*-octane conversion. Similar phenomenon was also observed for ZSM-12 [30] and Pt-Modernite [31] catalysts where the catalytic activity of the catalyst decreased with an increase in Si/Al ratio, which corresponds to the decrease in the acid sites density with increasing Si/Al ratio.

Since the Ir/Pt-HZSM5 with Si/Al ratio of 23 showed highest activity towards *n*-pentane isomerization, this catalyst was used in the subsequent studies of RSM.

3.2. RSM analysis

RSM is a method to determine the optimum condition of the process, and it allows users to gather large amounts of information from a small number of experiments. It is also possible to observe the relationships between variables and responses, and has been successfully applied for a wide range of chemical reactions involving more than one response [32,33]. Based on the RSM analysis, the quadratic model for the *n*-pentane conversion, isopentane selectivity and isopentane yield are presented in Eqs. (6)–(8):

$$Y_1 = -11730.4533 + 1.9095X_1 - 2.1762X_2 + 39.2484X_3 + 0.3923X_4 + 0.0049X_1X_2 - 0.0002X_1X_3 + 0.0001X_1X_4 - 0.0029X_2X_3 - 0.0005X_2X_4 - 0.0008X_3X_4 - 0.0013X_1^2 + 0.0121X_2^2 - 0.0344X_3^2 - 0.0001X_4^2 \quad (6)$$

$$Y_2 = -6401.4495 + 4.9904X_1 - 57.9955X_2 + 18.2130X_3 + 0.3051X_4 + 0.0301X_1X_2 - 0.0057X_1X_3 - 0.0003X_1X_4 + 0.0709X_2X_3 + 0.0030X_2X_4 + 0.0002X_3X_4 - 0.0014X_1^2 - 0.2046X_2^2 - 0.0138X_3^2 - 0.0002X_4^2 \quad (7)$$

$$Y_3 = -15299.7525 + 4.5847X_1 - 35.6623X_2 + 50.2891X_3 - 0.3628X_4 + 0.0191X_1X_2 - 0.0039X_1X_3 + 0.0002X_1X_4 + 0.0435X_2X_3 + 0.0001X_2X_4 - 0.0006X_3X_4 - 0.0019X_1^2 - 0.1082X_2^2 - 0.0427X_3^2 + 0.0005X_4^2 \quad (8)$$

where Y_1, Y_2 and Y_3 are the predicted percentage of *n*-pentane conversion, isopentane selectivity and isopentane yield, respectively.

Fig. 4 compares the observed values of *n*-pentane conversion, isopentane selectivity and isopentane yield with the predicted values obtained from Eqs. (6)–(8), respectively. The coefficient of determination (R^2) value for *n*-pentane conversion (Fig. 4A) is 0.9962 indicating 99.62% of the variability in the data is accounted to the model. Meanwhile, for isopentane selectivity (Fig. 4B) and isopentane yield (Fig. 4C) the R^2 values are 0.9801 and 0.9865 indicating that most of the variation of data can be explained by the model. According to Haaland [34], the empirical model is adequate to explain most of the variability in the essay reading which should be at least 0.75 or greater. The analysis of variance (ANOVA) in Table 3 shows that the *F*-value for *n*-pentane conversion, isopentane selectivity and isopentane yield are larger than the tabulated *F*-value ($F_{0.05}$ = 2.74). It can be concluded that the model obtained from Eqs. (6)–(8) give good prediction at 5% level of significance.

Fig. 5 demonstrates the *t*-distribution values in a Pareto chart and the corresponding *p*-values of the variables in Eqs. (6)–(8). The *p*-values serve as a tool to check the significance of each coefficient. The corresponding coefficient with smaller *p*-value or the greater magnitude of *t*-value donates more significant into the model. As illustrated in Fig. 5, the largest effect on *n*-pentane conversion, isopentane selectivity and isopentane yield is the linear term of reaction temperature (X_3), with the smallest *p*-value (0.000000, 0.000000, 0.000000) and largest *t*-value (47.7260, −13.0399, 17.1264) at 95% significant level, respectively. For *n*-pentane conversion, quadratic term of reaction temperature (X_3^2), linear term of treatment time (X_2), linear term of treatment temperature (X_1) and quadratic term of treatment temperature (X_1^2) could also be regarded as significant factors in affecting the *n*-pentane conversion due to the large *t*-value of −15.2188, −3.4092, −2.4932, and −2.3778, respectively. Meanwhile, for isopentane selectivity, the interaction term of treatment time and reaction temperature (X_2X_3), linear term of treatment time (X_2), linear term of treatment temperature (X_1), interaction term of treatment temperature and treatment time (X_1X_2), interaction term of treatment temperature and reaction temperature (X_1X_3) and quadratic term of reaction temperature (X_3^2) are significant at 95% significant level which is clearly indicated by larger *t*-value (8.4120, 8.2686, −7.8286, 7.1313, −6.7482, −3.2789) as compared to other variable terms. For isopentane yield, quadratic term of reaction temperature (X_3^2), linear term of treatment temperature (X_1), interaction term of treatment time and reaction temperature (X_2X_3), interaction term of treatment temperature and reaction temperature (X_1X_3), interaction term of treatment temperature and treatment time (X_1X_2) and linear term of treatment time (X_2) were also considered as significant factors in affecting the isopentane yield which can be seen from comparably large *t*-value of the respective variable terms (−11.0055, −6.4383, 5.6061, −4.9897, 4.9195, and 4.0594). The rest of factors could be considered less significant to affect the *n*-pentane conversion as their *p*-value higher than 0.05.

The response surfaces and contour plot are generally used to evaluate the relationships between parameters and to predict the result under given conditions. However, it is complicated to analyze the interaction between parameters in this study due to the presence of many interaction terms. Instead, the response surfaces and contour plot were used for optimizing the conditions of the

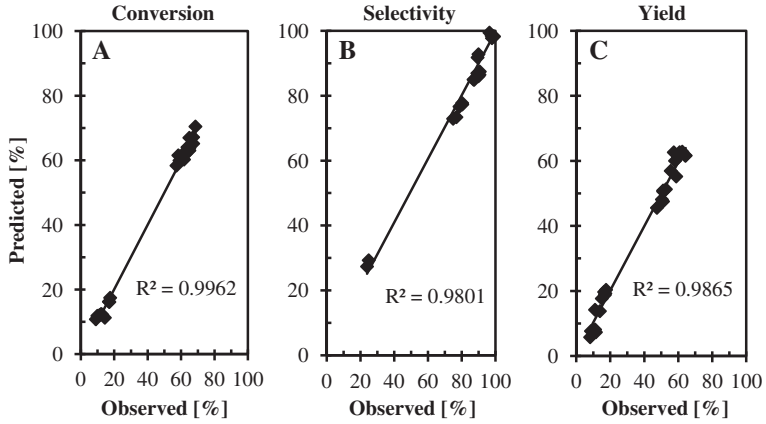

Fig. 4. Parity plot for the observed and predicted (A) *n*-pentane conversion, (B) isopentane selectivity and (C) isopentane yield.

Table 3
ANOVA for *n*-pentane conversion, *n*-pentane selectivity, *n*-pentane yield models.

Sources	Sum of squares (SS)	Degree of freedom (d.f.)	Mean square (MS)	*F*-value	$F_{0.05}$
n-Pentane conversion					
Regression (SSR)	14853.22	14	1060.94	207.62	>2.74
Residual	56.16	11	5.11		
Total (SST)	14909.38	25			
Isopentanes electivity					
Regression (SSR)	9613.95	14	686.71	38.62	>2.74
Residual	195.55	11	17.78		
Total (SST)	9809.50	25			
Isopentane yield					
Regression (SSR)	12086.56	14	863.33	57.29	>2.74
Residual	165.75	11	15.07		
Total (SST)	12252.31	25			

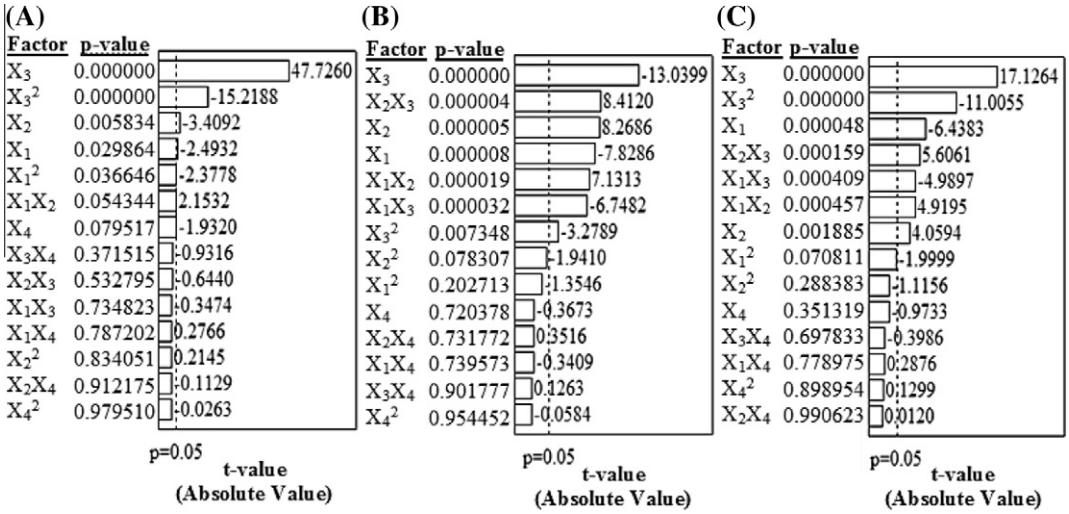

Fig. 5. Pareto chart and *p*-values of (A) *n*-pentane conversion, (B) isopentane selectivity and (C) isopentane yield.

n-pentane isomerization over Ir/Pt-HZSM5. In this paper, only isopentane yield is optimized since the value for the yield is the product of the *n*-pentane conversion and isopentane selectivity. Six RSM 3-D plots between four parameters were constructed for isopentane yield model (Fig. 6), and they were plotted in function of two of factors while the others were maintained constant at their mean levels. The interaction between the corresponding variables was negligible when the contour of response surface was circular. On the contrary, the interactions between the relevant variables were significant when the contour of response surfaces was elliptical. It is interesting to note that all the contour plots in Fig. 6 were elliptical indicating the significant interaction effects between the parameters studied.

Fig. 6A shows the response surface plot showing the effects of treatment temperature and treatment time on isopentane yield. From the analysis of the response surface plot, treatment temper-

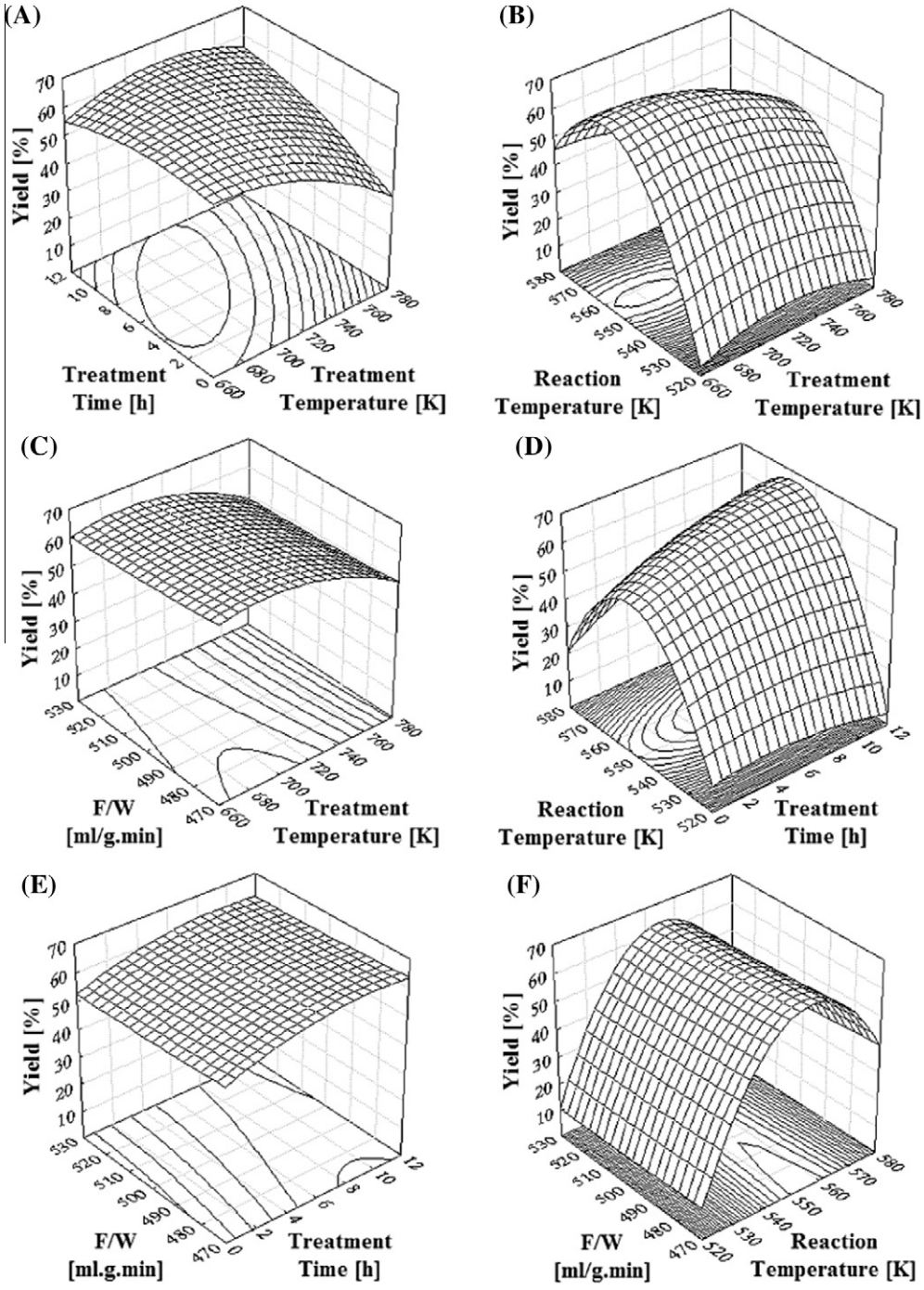

Fig. 6. Response surface plot of the combined (A) treatment temperature and treatment time; (B) treatment temperature and reaction temperature; (C) treatment temperature and *F*/*W*; (D) treatment time and reaction temperature; (E) treatment time and *F*/*W*; (F) reaction temperature and *F*/*W* on isopentane yield.

ature exhibited more significant influence on the response surface in comparison to treatment time, which also can be explained by the Pareto chart (Fig. 5C) showing larger *t*-value of treatment temperature (−6.4383) as compared to the treatment time (4.0594). An increase in the treatment temperature resulted to an increase in yield of isopentane, passing through a maximum around 723 K and decrease at higher temperature. This behavior may be related to the changes in the number of surface metal atoms due to an increase in the treatment temperature. Based on the study reported by Yoshioka et al. [35] for bimetallic catalyst, an increase in the treatment temperature leads to an increase in the number of surface metal atoms, reaching a maximum at 723 K and a decrease at higher temperatures. According to the concept of "hydrogen spillover phenomenon", hydrogen molecules are dissociatively adsorbed on metal sites to form hydrogen atoms, followed by the release of electrons near to the coordination unsaturated metal cations forming protonic acid sites, which play an important role in isomerization process. Thus an increase in metal sites will resulted to an increase in isomerization process. Fig. 6B represents the effects of treatment temperature and reaction temperature on isopentane yield. The increment of treatment temperature affected the isopentane yield slightly. Whereas, isopentane yield significantly increase with increasing reaction temperature and slightly decreased after reached the maximum, indicating the con-

sumption of the isomerized products in consecutive cracking reactions at higher temperatures. It is well known that the isomerization reaction is controlled by the thermodynamic equilibrium, where lower temperatures shift the equilibrium towards the formation of iso-paraffins, while higher temperatures shift the equilibrium towards cracking products [36]. The effects of treatment temperature and *F*/*W* on the yield of isopentane are shown in Fig. 6C. This figure indicated that the interaction of treatment temperature and *F*/*W* was not significant. Fig. 6D represents the effects of treatment time and reaction temperature on the isopentane yield. The effect of treatment time on the isopentane yield was slight, while the isopentane yield was significantly affected by reaction temperature. The significant effect of reaction temperature on the isopentane yield can be explained by the larger *t*-value of reaction temperature (17.1264) as compared to treatment time (4.0594) (Fig. 5C). At a constant treatment time, it was clear that an increase of reaction temperature evidently increased the yield of isopentane, reached the maximum around 548 K and decreased at higher temperature. This result is consistent with the catalytic testing study of Ir/Pt-HZSM5 at different reaction temperature of 473–623 K (not shown). A change in the yield of isopentane at higher temperature is related to the formation of cracking products, in which the formation of cracking products was almost zero at lower temperature (<553 K) and increased at higher temperature. Fig. 6E shows the effects of treatment time and *F*/*W* on the yield of isopentane. No significant changes were observed in the response surface plot indicating the interaction of treatment time and *F*/*W* was not significant. Fig. 6F shows the effects of different reaction temperature and *F*/*W* on the isopentane yield. From the analysis of response surface plot, reaction temperature exhibited significant influence on the response surface in comparison to *F*/*W*, which also can be clarified by the larger *t*-value of reaction temperature (17.1264) as compared to *F*/*W* (−0.9733) (Fig. 5C). A gradual rise in the yield of isopentane was seen with the increase in the reaction temperature. However after reached the maximum, the yield of isopentane slightly decreases with increasing reaction temperature. At constant reaction temperature, the effect of *F*/*W* on the yield of isopentane was almost negligible. All the parameters studied were found to affect the isomerization of *n*-pentane. However, from the analysis, it appears that reaction temperature plays the dominant factor in the yield of isopentane may be due to its strong relation with the formation of iso-paraffins. Additionally, it can be explained by the largest *t*-value of reaction temperature (17.1264) (Fig. 5C), which indicating most significant effect into the yield of isopentane.

The optimum isopentane yield was predicted from the response surface analysis and the predicted optimum isopentane yield is 61.9% at operating treatment temperature of 723 K, treatment time of 6 h, reaction temperature of 548 K and *F*/*W* of 500 ml g^{-1} min^{-1}. Additional experiment was carried out to validate the optimization result obtained by response surface analysis. The experimental and predicted isopentane yield at optimum condition is shown in Table 4. The *n*-pentane conversion and isopentane selectivity at the same condition are also predicted, as tabulated in the same table. The differences between the predicted and observed values are 1.7%, 0.8%, and 2.5% for *n*-pentane conversion, isopentane selectivity and isopentane yield. The errors were considered small as the observed values are within the 5% level of significance. The apparent activation energy of Ir/Pt-HZSM5 for reaction temperature at 473–533 K was 81.5 kJ/mol (Fig. 7).

3.3. Formation of coke deposits

Fig. 8A shows the isomerization of *n*-pentane on Ir/Pt-HZSM5 at optimum condition (treatment temperature of 723 K, treatment time of 6 h, reaction temperature of 548 K and *F*/*W* of 500 ml g^{-1} min^{-1}) in microcatalytic pulse reactor. In this experiment, the carrier gas was sequentially switched from hydrogen to nitrogen and switch back to hydrogen in order to examine the promotive effect of hydrogen and formation of coke deposits on Ir/Pt-HZSM5. In the first ten doses under a hydrogen stream, Ir/Pt-HZSM5 exhibited high activity for *n*-pentane isomerization in which the *n*-pentane conversion and isopentane yield reached 64% and 63%, respectively. However, the activity of the catalyst decreased markedly and close to zero after the hydrogen carrier gas was switched to nitrogen. The decrease in the catalytic activity after switching the carrier gas to nitrogen was due to the gradual exhaustion of adsorbed hydrogen (protonic acid sites) on the surface of catalyst. The absence of molecular hydrogen may prevent the formation of protonic acid sites, resulting in the inhibition of isomerization. The activity of Ir/Pt-HZSM5 recovered slowly with the pulse number when the carrier gas was switched back to the hydrogen. Although the activity did not recover completely after switching back to the hydrogen, a promoting effect of hydrogen was observed on Ir/Pt-HZSM5 catalyst. Deactivation of Ir/Pt-HZSM5 may be caused by the presence of coke deposits during the reaction in a nitrogen stream and may be occurs through the three following modes: (i) limitation of the access of *n*-pentane to the active sites, (ii) blockage of the access to the sites of the cavities (or channel intersections) in which the coke molecules are located and (iii) blockage of the access to the sites of the pores in which there are no coke molecules.

Several research groups have reported on the positive effect of hydrogen carrier gas in enhancement of the isomerization process. In general, it was concluded that hydrogen plays an important roles in the formation of active sites and inhibition of coke forma-

Table 4
Comparison between predicted and observed responses at the optimum condition obtained from RSM.

	Predicted value (%)	Observed value (%)	Error (%)
Conversion	63.0	64.1	1.7
Selectivity	98.2	99.0	0.8
Yield	61.9	63.5	2.5

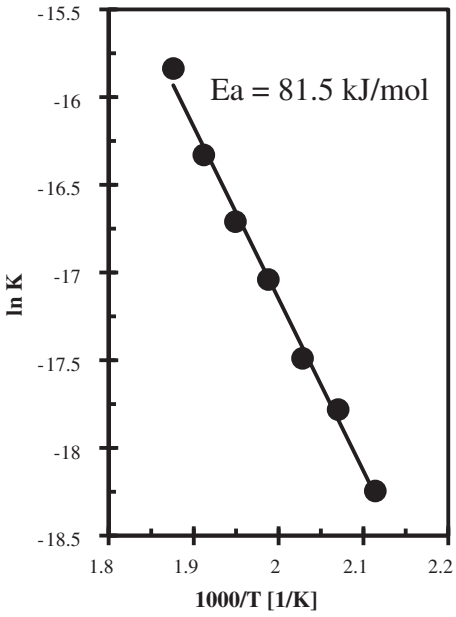

Fig. 7. Arrhenius plot for *n*-pentane isomerization over Ir/Pt-HZSM5 in the temperature range 473–533 K.

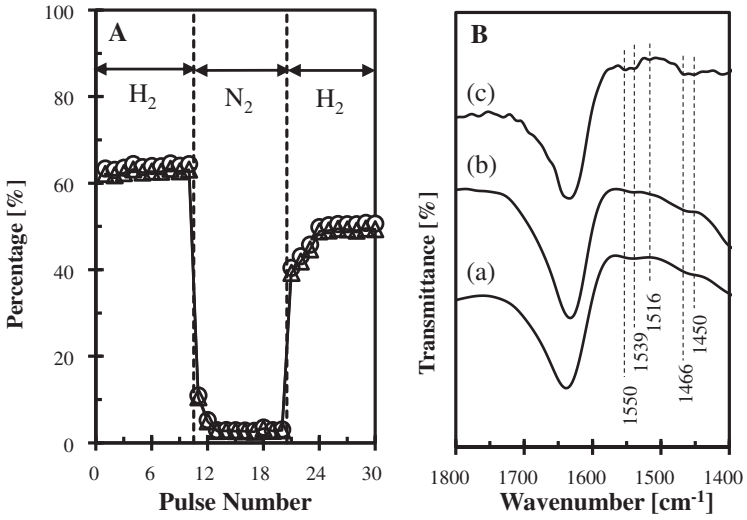

Fig. 8. (A) *n*-pentane conversion (○) and isopentane yield (Δ) over Ir/Pt-HZSM5 at 548 K under hydrogen and nitrogen stream. (B) FTIR spectra of Ir/Pt-HZSM5; (a) fresh catalyst, (b) after isomerization in the presence of hydrogen and (c) after isomerization in the presence of nitrogen.

tion on the catalyst surface [37,38]. Fujimoto et al. [39] studied the hydroconversion of *n*-pentane over hybrid catalysts under hydrogen and nitrogen atmospheres. In the absence of hydrogen, the conversion of *n*-pentane was dramatically reduced and an oligomerization reaction became dominant. They suggested that the spillover hydrogen play an important role in *n*-alkane hydroconversion. In addition, our research groups have reported the promotive effect of hydrogen on the isomerization of *n*-pentane over Zn/HZSM5 [40] and Zn-HBEA [5]. For both catalysts, the selectivity to isopentane was close to zero for the isomerization in the nitrogen stream due to the gradually exhaustion of protonic acid sites and formation of coke deposits on the surface of catalyst. It was suggested that strong Lewis acid sites in the absence of hydrogen may become active sites for the formation of dehydrogenated carbonaceous species, which considered being a precursor of coke on the catalyst surface.

The presence of coke deposits on the surface of Ir/Pt-HZSM5 was observed by IR spectroscopy. Fig. 8B shows the IR spectra of fresh Ir/Pt-HZSM5 and used Ir/Pt-HZSM5 catalysts under hydrogen and nitrogen stream. The IR spectra of used Ir/Pt-HZSM5 under nitrogen stream shows the development of several bands at 1570, 1550, 1539, 1516,1486, 1466, 1450, 1430 and 1412 cm^{-1}. The band at 1570, 1550 and 1539 cm^{-1} are widely reported to be assignable to coke [41], while the band at 1516 cm^{-1} is assigned to alkenylcarbenium ions [42]. The band at 1486 cm^{-1} is assigned to the C–H bond deformation vibrations of $–CH_3$ [41], whereas the band at 1466 cm^{-1} is assigned to $–CH_2$ groups [43]. In addition, the bands at 1450, 1430 and 1412 cm^{-1} are attributed to branched alkanes [44,45]. All of these bands indicate a substantial amount of coke and carbonaceous species formed in the absence of hydrogen. The presence of coke deposits on the surface of catalyst during the reaction under nitrogen stream was also observed on Zn-HBEA as reported by Kamarudin et al. [5]. IR spectra of used Zn-HBEA under nitrogen stream showed the development of several bands which associated to coke and carbonaceous species. In addition, TGA analysis of used Zn-HBEA under nitrogen stream confirmed the formation of coke in the surface of catalyst.

4. Conclusion

The study of the effect of Si/Al ratio showed that increase in the Si/Al ratio increased the percentage crystallinity of the catalyst and decreased the number of strong Brönsted and Lewis acid sites which led to decrease the catalytic activity of Ir/Pt-HZSM5 towards *n*-pentane isomerization. A decrease in the strong acid sites due to the decrease in the both tetrahedral and octahedral aluminum in the zeolite. Thus, Ir/Pt-HZSM5 with Si/Al ratio of 23 showed highest activity towards *n*-pentane isomerization.

Since the Ir/Pt-HZSM5 with Si/Al ratio of 23 showed highest activity towards *n*-pentane isomerization, the operating condition for this catalyst was further optimized using response surface methodology (RSM). The Pareto chart indicated that the variable with the largest effect was the linear term of reaction temperature (X_3) followed by quadratic term and linear interaction of X_3. The predicted value for the *n*-pentane conversion, isopentane selectivity and isopentane yield at optimum condition was 63.0%, 98.2% and 61.9%, respectively, with relatively small errors (1.7%, 0.8%, and 2.5%). Therefore, the optimum condition for *n*-pentane isomerization over Ir/Pt-HZSM5 was at treatment temperature of 723 K, treatment time of 6 h, reaction temperature of 548 K and *F*/*W* of 500 ml g^{-1} min^{-1}.

Acknowledgements

This work was supported by the Research University Grant, Universiti Teknologi Malaysia No. 00H95. Our gratitude also goes to Universiti Malaysia Pahang for the award of Skim Fellowship Universiti Malaysia (Herma Dina Setiabudi) and the Hitachi Scholarship Foundation for the Gas Chromatograph Instruments Grant.

References

[1] S. Triwahyono, T. Yamada, H. Hattori, Effects of Na addition, pyridine preadsorption, and water preadsorption on the hydrogen adsorption property of $Pt/SO_4^2 – ZrO_2$, Catal. Lett. 85 (2003) 109–115.
[2] S. Triwahyono, A.A. Jalil, H. Hattori, Study of hydrogen adsorption on $Pt/WO_3–ZrO_2$ through Pt sites, J. Nat. Gas Chem. 16 (2007) 252–257.
[3] C.G. Volkova, S.I. Reshetnikov, L.N. Shkuratova, A.A. Budneva, E.A. Paukshtis, N-Hexane skeletal isomerization over sulfated zirconia catalysts with different Lewis acidity, Chem. Eng. J. 134 (2007) 106–110.
[4] A. Corma, D. Kumar, Possibilities of mesoporous materials in catalysis, Stud. Surf. Sci. Catal. 117 (1998) 201–222.
[5] N.H. N Kamarudin, A.A. Jalil, S. Triwahyono, R.R. Mukti, M.A.A. Aziz, H.D. Setiabudi, M.N.M. Muhid, H. Hamdan, Interaction of Zn2+ with extraframe work aluminum in HBEA zeolite and its role in enhancing *n*-pentane isomerization, Appl. Catal. A: Gen. 431–432 (2012) 104–112.
[6] M.A.A. Aziz, N.H. N Kamarudin, H.D. Setiabudi, H. Hamdan, A.A. Jalil, S. Triwahyono, Negative effect of Ni on PtHY in *n*-pentane isomerization evidenced by IR and ESR studies, J. Nat. Gas Chem. 21 (2012) 29–36.
[7] J. Weitkamp, P.A. Jacobs, J.A. Martens, Isomerization and hydrocracking of C9 through C16 *n*-alkanes on Pt/HZSM-5 zeolite, Appl. Catal. 8 (1983) 123–141.

[8] S. Triwahyono, A.A. Jalil, M. Musthofa, Generation of protonic acid sites from pentane on the surfaces of $Pt/SO_4^2 - ZrO_2$ and Zn/H-ZSM5 evidenced by IR study of adsorbed pyridine, Appl. Catal. A: Gen. 372 (2010) 90–93.
[9] K.L. Yeung, E.E. Wolf, A scanning tunnelling microscopy study of the platinum catalysts particles supported on graphite, J. Vac. Sci. Technol., B 9 (1991) 798–803.
[10] K.L. Yeung, E.E. Wolf, Scanning tunnelling microscopy studies of size and morphology of Pt/graphite catalysts, J. Catal. 135 (1992) 13–26.
[11] J.H. Sinfelt, US Patent 3,953,368, 1976.
[12] M.J. Dees, V. Ponec, On the influence of sulfur on the platinum/iridium bimetallic catalysts in *n*-hexane/hydrogen reactions, J. Catal. 115 (1989) 347–355.
[13] O.B. Yang, S.I. Woo, Characterization and catalytic properties of Pt-Ir small bimetallic cluster in NaY, in: L. Guczi, F. Solymosi, P. Tetenyi (Eds.), New Frontiers in Catalysis – Proceeding of the 10th International Congress on Catalysis, vol. 75, Elsevier, Amsterdam, 1993, pp. 671–680.
[14] A.K. Aboul-Gheit, A.E. Awadallah, N.A.K. Aboul-Gheit, E.S.A. Solyman, M.A. Abdel-Aaty, Effect of hydrochlorination and hydrofluorination of Pt/H-ZSM-5 and Pt-Ir/H-ZSM-5 catalysts for *n*-hexane hydroconversion, Appl. Catal. A: Gen. 334 (2008) 304–310.
[15] H.D. Setiabudi, A.A. Jalil, S. Triwahyono, N.H.N. Kamarudin, R.R. Mukti, IR study of iridium bonded to perturbed silanol groups of Pt-HZSM5 for *n*-pentane isomerization, Appl. Catal. A: Gen. 417–418 (2012) 190–199.
[16] H.D. Setiabudi, A.A. Jalil, S. Triwahyono, Ir/Pt-HZSM5 for *n*-pentane isomerization: effect of iridium loading on the properties and catalytic activity, J. Catal. 294 (2012) 128–135.
[17] S. Triwahyono, Z. Abdullah, A.A. Jalil, The effect of sulfate ion on the isomerization of *n*-butane to isobutane, J. Nat. Gas Chem. 15 (2006) 247–252.
[18] H.D. Setiabudi, S. Triwahyono, A.A. Jalil, N.H.N. Kamarudin, M.A.A. Aziz, Effect of iridium loading on HZSM-5 for isomerization of *n*-heptane, J. Nat. Gas Chem. 20 (2011) 477–482.
[19] D.C. Montgomery, Design and analysis of experiments, fourth ed., John Wiley & Sons, New York, 1996.
[20] M.M.J. Treacy, J.B. Higgins, Collection of Simulated XRD Powder Patterns for Zeolites, fourth ed., Elsevier, Amsterdam, 2001.
[21] A. Abraham, S.H. Lee, C.H. Shin, S.B. Hong, R. Prins, J.A. van Bokhoven, Influence of framewok silicon to aluminium ratio on aluminium coordination and distribution in zeolite Beta investigated by 27Al MAS and 27Al MQ MAS NMR, Phys. Chem. Chem. Phys. 6 (2004) 3031–3036.
[22] J. Lu, Z. Zhao, C. Xu, A. Duan, X. Wang, P. Zhang, Catalytic cracking of isobutene over HZSM-5, FeHZSM-5 and CrHZSM-5 catalysts with different SiO_2/Al_2O_3 ratios, J. Porous Mater. 15 (2008) 213–220.
[23] K.M. Reddy, C. Song, Synthesis of mesoporous molecular sieves: influence of aluminium source on Al incorporation in MCM-41, Catal. Lett. 36 (1996) 103–109.
[24] C. Morterra, G. Cerrato, G. Meligrana, Revisiting the use of 2,6-dimethylpyridine adsorption as a probe for the acidic properties of metal oxides, Langmuir 17 (2001) 7053–7060.
[25] W.O. Haag, R.M. Lago, P.B. Weisz, The active site of acidic aluminosilicate catalysts, Nature 309 (1984) 589–591.
[26] P.B. Weisz, Remarkable active site: Al in SiO_2, Ind. Eng. Chem. Fundam. 25 (1986) 53–58.
[27] L. Shirazi, E. Jamshidi, M.R. Ghasemi, The effect of Si/Al ratio of ZSM-5 zeolite on its morphology, acidity and crystal size, Cryst. Res. Technol. 43 (12) (2008) 1300–1306.
[28] V.R. Choudhary, K. Mantri, C. Sivadinarayana, Influence of zeolite factors affecting zeolitic acidity on the propane aromatization activity and selectivity of Ga/H-ZSM-5, Microporous Mesoporous Mater. 37 (2000) 1–8.
[29] A. De Lucas, M.J. Ramos, F. Dorado, P. Sánchez, J.L. Valverde, Influence of the Si/Al ratio in the hydroisomerization of *n*-octane over platinum and palladium beta zeolite-based catalysts with or without binder, Appl. Catal. A: Gen. 289 (2005) 205–213.
[30] W. Zhang, P.G. Smirniotis, Effect of zeolite structure and acidity on the product selectivity and reaction mechanism for *n*-octane hydroisomerization and hydrocracking, J. Catal. 182 (1999) 400–416.
[31] M. Guisnet, V. Fouche, M. Belloum, J.P. Bournonville, C. Travers, Isomerization of *n*-hexane on platinum dealuminated mordenite catalysts I. Influence of the silicon-to-aluminum ratio of the zeolites, Appl. Catal. 71 (1991) 283–293.
[32] S. Chatterjee, A. Kumar, S. Basu, S. Dutta, Application of response surface methodology for methylene blue dye removal from aqueous solution using low cost adsorbent, Chem. Eng. J. 181–182 (2012) 289–299.
[33] R. Kumar, P. Pal, Response surface-optimized Fenton's pre-treatment for chemical precipitation of struvite and recycling of water through downstream nanofiltration, Chem. Eng. J. 210 (2012) 33–44.
[34] P.D. Haaland, Experimental Design in Biotechnology, Marcel Dekker Inc., New York, 1989.
[35] C.M.N. Yoshioka, M.H. Jordão, D. Zanchet, T.F. Garetto, D. Cardoso, A new activation process of bimetallic catalysts and application to the *n*-hexane isomerization, Appl. Catal. A: Gen. 355 (2009) 20–26.
[36] P.J. Kuchar, J.C. Bricker, M.E. Reno, R.S. Haizman, Paraffin isomerization innovations, Fuel Proc. Technol. 35 (1993) 183–200.
[37] T. Hosoi, T. Shimadzu, S. Ito, S. Baba, H. Takaoka, T. Imai and N. Yokoyama, Characterization and C5/C6 isomerization activity of solid superacid $(Pt/SO_4^2 - /ZrO_2)$, in: Prep. Symp. Div. Petro. Chem. Am. Chem. Soc., Los Angeles, 1988, pp. 562–567.
[38] H. Hattori, T. Shishido, Molecular hydrogen-originated protonic acid sites as active site on solid acid catalyst, Catal. Surv. Jpn. 1 (1997) 205–213.
[39] K. Fujimoto, K. Maeda, K. Aimoto, Hydroisomerization of *n*-pentane over hybrid catalysts containing a supported hydrogenation catalyst, Appl. Catal. A: Gen. 91 (1992) 81–86.
[40] S. Triwahyono, A.A. Jalil, R.R. Mukti, M. Musthofa, N.A.M. Razali, M.A.A. Aziz, Hydrogen spillover behaviour of Zn/HZSM-5 showing catalytically active protonic acid sites in the isomerization of *n*-pentane, Appl. Catal. A: Gen. 407 (2011) 91–99.
[41] H.G. Karge, Coke formation on zeolites, in: H. van Bekkum, E.M. Flanigen, P.A. Jacobs, J.C. Jansen (Eds.), Introduction to Zeolite Science and Practice, Elsevier, Amsterdam, 2001, pp. 707–746.
[42] S. Yang, J.N. Kondo, K. Domen, Formation of stable alkenylcarbenium ions in high yield by adsorption of 1-methylcyclopentane on zeolite Y at low temperature, Chem. Commun. (2001) 2008–2009.
[43] J.N. Kondo, S. Yang, Q. Zhu, S. Inagaki, K. Domen, In situ infrared study of *n*-heptane isomerization over Pt/H-beta zeolites, J. Catal. 248 (2007) 53–59.
[44] A. De Lucas, R. Canizares, A. Durán, A. Carrero, Coke formation, location, nature and regeneration on dealuminated HZSM-5 type zeolites, Appl. Catal. A: Gen. 156 (1997) 299–317.
[45] M.S. Renzini, L.C. Lerici, U. Sedran, L.B. Pierella, Stability of ZSM-11 and BETA zeolites during the catalytic cracking of low-density polyethylene, J. Anal. Appl. Pyrol. 92 (2011) 450–455.